Perinasal Imaging of Physiological Stress and Its Affective Potential

Dvijesh Shastri, *Member*, *IEEE*, Manos Papadakis, Panagiotis Tsiamyrtzis, Barbara Bass, and Ioannis Pavlidis, *Senior Member*, *IEEE*

Abstract—In this paper, we present a novel framework for quantifying physiological stress at a distance via thermal imaging. The method captures stress-induced neurophysiological responses on the perinasal area that manifest as transient perspiration. We have developed two algorithms to extract the perspiratory signals from the thermophysiological imagery. One is based on morphology and is computationally efficient, while the other is based on spatial isotropic wavelets and is flexible; both require the support of a reliable facial tracker. We validated the two algorithms against the clinical standard in a controlled lab experiment where orienting responses were invoked on $n = 18$ subjects via auditory stimuli. Then, we used the validated algorithms to quantify stress of surgeons ($n = 24$) as they were performing suturing drills during inanimate laparoscopic training. This is a field application where the new methodology shines. It allows nonobtrusive monitoring of individuals who are naturally challenged with a task that is localized in space and requires directional attention. Both algorithms associate high stress levels with novice surgeons, while low stress levels are associated with experienced surgeons, raising the possibility for an affective measure (stress) to assist in efficacy determination. It is a clear indication of the methodology's promise and potential.

Index Terms—Physiological stress, thermal imaging, image morphology, isotropic wavelets

1 Introduction

Stress is an ever-present mechanism that helps the human body to cope with perceived or real threats or challenges [1]. Due to its ubiquitous and semi-stochastic nature, stress is very difficult to measure and understand. Things are further complicated because the measurement process itself generates stress, thus altering results.

Stress is suspected to play a pivotal role in challenging tasks. Examples of such tasks include surgical training, pilot training, training of robot teleoperators, and others. In all these cases of critical dexterous tasking, there are open issues associated with the effect of stress on human performance, the effectiveness of training regimes, and the certification of efficacy. Please note that due to the criticality of these application areas, any progress on the open issues is likely to have significant societal impact. Up to now, thorough and objective stress studies of this sort were difficult or impossible. Psychometric scoring [2], [3], [4], which is often used in stress studies, is subjective, while facial observations [5] provide useful but qualitative indicators. Physiological measurements are quantifiable and more objective, but have been considered obtrusive.

Broadly speaking, researchers are divided into two schools for measuring physiological manifestations of stress: One is focused on measuring brain activity [6] through functional Magnetic Resonance Imaging (fMRI) or electroencephalography (EEG). The other is focused on measuring physiological responses on the body through contact sensors [7]. These include piezoelectric probes for measuring pulsation, thoracic strap transducers for measuring breathing, and Electrodermal Activity (EDA) probes for measuring perspiratory responses on the fingers [8]. Recently, a more user-friendly form of EDA sensing has come into being, the Q sensor, which is worn as a bracelet and reportedly produces signals that correlate well with the finger EDA signals [9].

Studying physiological stress via the brain activity that generates it has profound value. Nevertheless, there are limitations as such studies are restricted by necessity to highly artificial experimental scenarios. Capturing peripheral bodily responses associated to stress provides more freedom at the expense of specificity. For example, transient perspiratory responses can be measured at various parts of the body with increasingly user-friendly technology, but they indicate arousal, which tracks stress only within certain contexts.

In [10], we showed that perspiratory responses on the fingers, precipitated by auditory stimuli, are concomitant to facial perspiratory responses centered on the maxillary area. In fact, the facial response extends throughout the perinasal region. Consequently, we postulated that orienting reactions (and hence stress within well-defined contexts) can be peripherally measured on the face instead of the fingers.

- *D. Shastri is with the Department of Computer and Mathematical Sciences, University of Houston-Downtown, One Main Street #S705, Houston, TX 77002. E-mail: shastrid@uhd.edu.*
- *M. Papadakis is with the Department of Mathematics, University of Houston, 651 Philip G. Hoffman Hall, Houston, TX 77204. E-mail: mpapadak@math.uh.edu.*
- *P. Tsiamyrtzis is with the Department of Statistics, Athens University of Economics and Business, 76 Patission Street, Athens 10434, Greece. E-mail: pt@aueb.gr.*
- *B. Bass is with the Department of Surgery, The Methodist Hospital, Suite 1661, 6550 Fannin Street, Houston, TX 77030. E-mail: bbass@tmhs.org.*
- *I. Pavlidis is with the Department of Computer Science, University of Houston, 501 Philip G. Hoffman Hall, Houston, TX 77204. E-mail: ipavlidis@uh.edu.*

Manuscript received 27 Feb. 2011; revised 15 Feb. 2012; accepted 12 Apr. 2012; published online 20 June 2012.
Recommended for acceptance by S.-W. Lee.
For information on obtaining reprints of this article, please send e-mail to: taffc@computer.org, and reference IEEECS Log Number TAFFC-2011-02-0015.
Digital Object Identifier no. 10.1109/T-AFFC.2012.13.

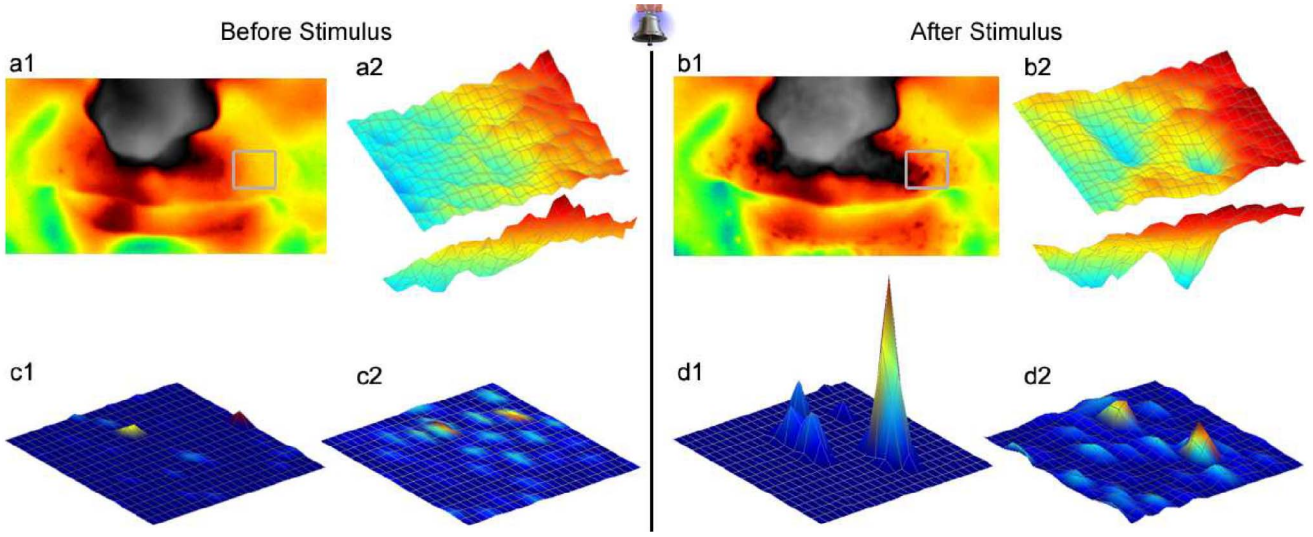

Fig. 1. (a1), (b1) Thermal image of a subject's face before and after an auditory startle stimulus; the gray rectangle delineates the region of interest. (a2), (b2) 3D thermal plots of ROI before and after stimulus. The smooth conic profiles of the emerging perspiration spots denote the gradual transition from a "cold" core to a "hot" surrounding background. (c1), (d1) and (c2), (d2) Nonnormalized 3D energy plots yielded by the morphological and wavelet extraction algorithms before and after stimulus.

We further suggested that this measurement could be done via thermal imaging, that is, in a contact-free manner. We offered no specific algorithmic method, however, to perform the measurement practically. Furthermore, our investigation was confined to a lab setting only and did not extend to any field studies.

In this paper, we report two different algorithms that reliably extract perspiratory signals from thermophysiological perinasal data captured via thermal imaging. One algorithm is based on image morphology, while the other is based on spatial isotropic wavelets. An appropriate tissue tracker which ameliorates the effect of motion supports the algorithms.

The characteristics of the two imaging methods are brought to the fore in a simulation study. Then, their performance is validated against EDA in a lab study, whereby orienting responses are evoked through auditory stimuli. Finally, the methods are applied to a representative field study where stress is measured in-situ during inanimate surgical training. The conclusions afforded by the extracted signals shed light on the nature and impact of stress in this critical activity.

2 Methodology

Perspiration is a physiological phenomenon with a clear thermal imprint. Hence, it can be captured through thermal imaging. When activated, perspiration pores lower locally thermal emission by absorbing latent heat. As a result, they appear as "cold" spots in the thermal imagery.

Perspiratory responses due to stress stimuli are not the same as perspiration produced during strenuous physical exercise. The major difference is in the time scale and extent of the phenomenon. Stress-induced perspiratory responses are transient (last a few seconds) and spread throughout the body, assuming high density in certain areas such as the fingers, the toes, and the maxillary region. Perspiration due to physical activity is a more sustained phenomenon and covers the body somewhat more uniformly. Also, the function of these two phenomena is quite different. Physical activity perspiration has a thermoregulatory role [11]. It is not clear what the role of transient stress-induced perspiration is. In all likelihood, it has a bioevolutionary explanation [12]. Our working hypothesis is that one of its aims is to enhance tactile and olfactory sensing in moments of threat while protecting probing sensors that may be in contact with a harmful environment.

Irrespective of the true origin of the response, this paper demonstrates that it can be quantified and used as a stress indicator. Figs. 1a1 and 1b1 show thermophysiological snapshots of a subject's perinasal response before and after an auditory startle stimulus. The resulting perspiration spots are characterized by somewhat fuzzy boundaries due to thermal diffusion; they also feature a distinct morphological pattern—a "cold" inner area transitioning to a "hot" surrounding background (see Figs. 1a2 and 1b2). Therefore, one option is to apply a morphology-based localization approach (see Figs. 1c1 and 1d1). An edge-based localization approach is not particularly attractive here due to boundary fuzziness.

The circular spots are clustered, inducing a high frequency spatial pattern of isotropic nature. Hence, another option is to apply 2D multiresolution wavelet analysis driven by isotropic filters (see Figs. 1c2 and 1d2). We developed appropriate isotropic filters from the ground up and proved their properties for that purpose.

2.1 Morphology-Based Signal Extraction

In facial thermal imagery, activated perspiration pores appear as small "cold" (dark) spots amidst substantial background clutter. The latter is the thermophysiological manifestation of the metabolic processes in the surrounding tissue. The morphological method of choice for bringing up dark ("cold") objects in an image is the black top-hat transformation [13]. However, due to the small target size and the background fuzziness, the standard black top-hat transformation does not work very well in our application. As can be seen in Fig. 2a, it yields inefficient background elimination and poor localization of the perspiration spots.

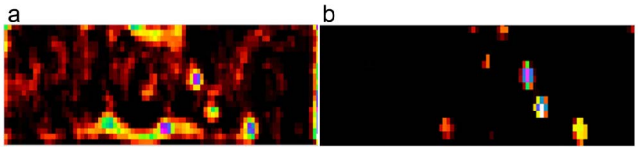

Fig. 2. (a) Output from the conventional black top-hat transformation method. (b) Output from the contour-based black top-hat transformation method.

The culprit is the structuring element; its filled nature proves to be too gross of a sculpting tool for the delicate job needed here. We opt instead to use a contour structuring element, which reportedly is a better choice for applications, such as ours [14].

Let f and S represent the thermal image of the perinasal region and the planar structuring element, respectively. Also let ∂S be the boundary of S determining the connectedness of S. Then, the contour-based black top hat transformation is defined as

$$BTH_{CB}(f) = O_B(f) - f, \tag{1}$$

where $O_B(f) = \max\{f, O_{CB}(f)\}$; $O_{CB}(f)$ denotes contour-based opening, which is defined as

$$O_{CB}(f) = (f \ominus \partial S) \oplus S, \tag{2}$$

where $\ominus$ and $\oplus$ denote an *erosion* and *dilation* operation [13], respectively.

The resultant region $f' = BTH_{CB}(f)$ brings to the fore the cold spots (perspiration activity). The contour-based black top-hat transformation is applied to every frame in the thermal clip to capture the evolution of the perspiration spots. The perspiration extraction algorithm is not affected by hot spots in the imagery; they are eliminated by the contour-based *erosion* operation. Fig. 2b shows an example of the method's superior performance and Fig. 3 depicts the algorithmic flow.

Finally, we compute the energy in the perinasal region of every thermal frame as follows:

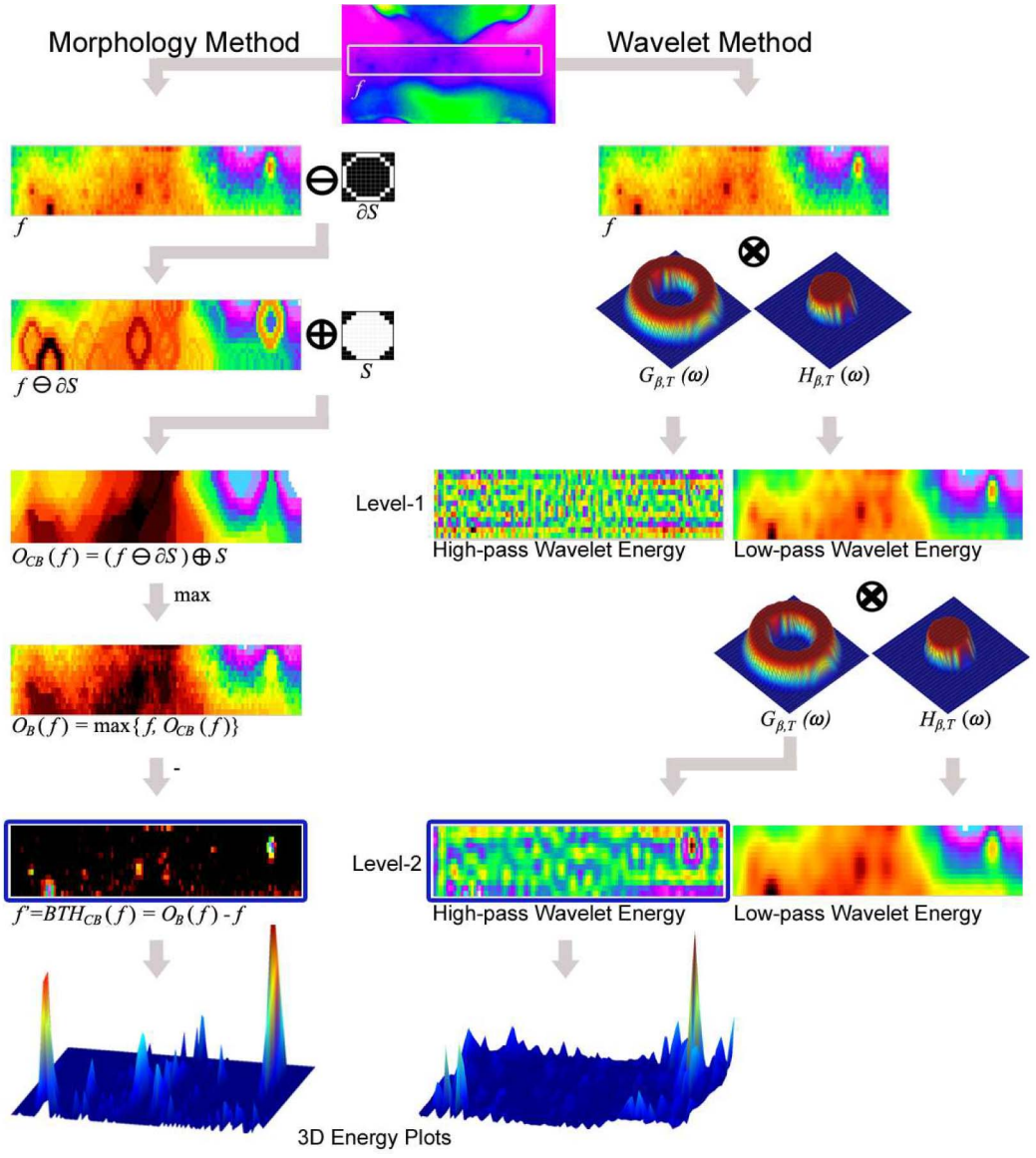

Fig. 3. Algorithmic flow in the morphology and wavelet-based methods. In the wavelet-based method, the transfer function of the low-pass filter is $H_{\beta,T}$ with $0.5(1+\beta)/T = 0.23$ and $\beta/T = 0.06$, while the transfer function of the high-pass filter is $H_{\beta,\frac{1}{2}}G_{\beta,T}$ with $0.5(1+\beta)/T = 0.23$ and $\beta/T = 0.06$.

$$E_M(f'(t_s)) = \frac{1}{N_c(f'(t_s))} \sum_{(m,n)} |f'(t_s)(m,n)|^2, \quad (3)$$

where t_s is the time at which the frame s is captured and $N_c(f'(t_s))$ is the number of detected cold spots at that time. Shift and rotation invariance of $E_M(f'(t_s))$ is very important as the projection of the face on the 2D-camera plane always shifts and rotates due to motion of the head. Thankfully, due to the isotropic nature of the structuring element, $E_M(f'(t_s))$ is both shift and rotation invariant. For a detailed discussion on invariant properties of morphological operators, the interested reader is referred to [15]. The evolution of $E_M(f'(t_s))$ produces an energy signal $\mathbf{E}_M$, which is indicative of perspiration activity in the perinasal area per the morphology method; for this reason we call it a perspiration signal. Furthermore, because we use this to quantify levels of stress, we also call it a stress signal.

2.2 Isotropic Wavelet-Based Signal Extraction

Each perspiration spot in facial thermal imagery is a patch that can be modeled as a stochastic texture with no prevailing directional characteristics. The texture of a perspiration patch is created by the spatiotemporal oscillation of its intensity values, which is higher than the oscillation of the intensity values in the surrounding region. Moreover, the perspiration patches are spatially and temporally transient as they appear and disappear following evolutionary curves with capacitive characteristics.

We want to use this locally oscillatory nondirectional texture of the perspiration patches to extract a numerical feature that will allow us to identify their presence. Furthermore, this numerical feature must not be influenced by the rigid motions (rotations and translations) of the facial patch; otherwise, the robustness of the method will be severely compromised. To extract such a numerical feature we use an image multiscale representation based on a new class of 2D-isotropic wavelet filters. The isotropy of these filters eliminates any directional bias that can compromise the detection of perspiration spots.

To clear any notational confusion, the Fourier transform $\hat{f}$ of a function $f \in L^1(\mathbb{R}^2)$ is defined by $\hat{f}(\omega) = \int_{\mathbb{R}^2} f(\mathbf{x}) e^{-2\pi i(\mathbf{x}\cdot\omega)} d\mathbf{x}$, where $\omega \in \mathbb{R}^2$; in accordance, the Nyquist frequency domain in 2D is the square $[-\frac{1}{2}, \frac{1}{2}) \times [-\frac{1}{2}, \frac{1}{2})$. Please note that f in this case represents the thermal image of the perinasal region.

The isotropic wavelet filters we use arise as low and high-pass filters of the Isotropic Multiresolution Analysis (IMRA) [16], [17]. Their transfer functions are radial inside the ball $B(0, 1/2)$ centered at the origin of the coordinate system of the frequency domain. More specifically, the transfer function of the low-pass filter, $H_{\beta,T}$, is given by

$$H_{\beta,T}(\boldsymbol{\omega}) = \begin{cases} 1, & |\boldsymbol{\omega}| \le \frac{1-\beta}{2T} \\ \frac{1}{2}\left[1 + cos\left(\frac{\pi T}{\beta}\left(|\boldsymbol{\omega}| - \frac{1-\beta}{2T}\right)\right)\right], & \frac{1-\beta}{2T} \le |\boldsymbol{\omega}| \le \frac{1+\beta}{2T} \\ 0, & \text{otherwise} \end{cases}$$

where $\omega = (\omega_1, \omega_2)$ and $|\omega_i| \le 1/2$, $i = 1, 2$. The parameter $\beta > 0$ determines the width β/T of the transition band, whereas $T > 0$ determines the cut-off frequency of the filter. The transfer function of the high-pass filter, $G_{\beta,T}$, is given by $G_{\beta,T}(\omega) = \sqrt{1 - H^2_{\beta,T}(\omega)}$, for all ω with $|\omega_i| \le 1/2$, $i = 1, 2$. The reader can easily observe that the lowering of the scale by one level can be done by using $2T$ instead of T. In fact,

$$H_{\beta,2T}(\omega) = H_{\beta,T}(2\omega), \quad |\omega_i| \le 1/2, i = 1, 2. \quad (4)$$

Fig. 3 depicts the high and low-pass filters used along with the entire algorithmic flow. Both filters have compact support and good band separation in the frequency domain. Therefore, they cannot be implemented by a filter with a finite number of filter taps. To circumvent this problem and optimize the fidelity of the radial filter design we apply the filter in the frequency domain by multiplying the Fourier transform of the image with the transfer function of the filter. This application is equivalent to implementing the filter with fast convolution. To fully exploit the radiality of the filter we need a sufficiently dense sampling grid. Typically the images we acquire have a sampling grid higher than 100×100. The same grid is used to compute the Fourier transform of the image. These denser sampling grids enable the almost radial approximations of the radial transfer functions $H_{\beta,T}$ and $G_{\beta,T}$.

These filters are referred to as analysis filters. They require an associated pair of synthesis filters that are used for the reconstruction Isotropic Wavelet Transform [17], [18]. In this paper, we do not use the reconstruction part of the transform. We only care to propose a numerical feature that will allow us to identify the presence of perspiration patches and thus to quantify perspiration. This feature is the mean energy per pixel $E_W(f(t_s))$ of the high-pass output of the second iteration of the Analysis Isotropic Wavelet Transform:

$$E_W(f(t_s)) = \frac{1}{N} \sum_{m,n} |(f(t_s) * h_{\beta,T} * g_{\beta,2T})(m,n)|^2, \quad (5)$$

where t_s is the time instance corresponding to frame s of the thermal sequence and N is the number of pixels in the perinasal Region of Interest (ROI). Interestingly, our analysis shows that $E_W(f(t_s))$ is not influenced by decimation up to a constant factor depending only on the decimation parameter. Shift and rotation invariance of $E_W(f(t_s))$ is very important as the projection of the face on the 2D-camera plane always shifts and rotates due to motion of the head (for proof see the Appendix, which can be found in the Computer Society Digital Library at http://doi.ieeecomputersociety.org/10.1109/T-AFFC.2012.13). The evolution of $E_W(f(t_s))$ produces an energy signal $\mathbf{E}_W$, which is indicative of the perspiration activity in the perinasal area per the wavelet method; for this reason, we call it a perspiration signal. Furthermore, because we use this to quantify levels of stress, we also call it a stress signal.

2.3 Tissue Tracking

To track perinasal tissue in thermal imaging, we use the tracker we reported in [19]. It can handle various head poses, partial occlusions, and thermal variations. On the initial frame, the user initiates the tracking algorithm by selecting the maxillary portion of the perinasal region. The tracker estimates the best matching block in the next frame of the thermal clip. Next, the morphology-based or wavelet-based algorithm is applied to compute the perspiration level. The tracking step, along with the physiological computation, is

iteratively implemented until the end of the thermal sequence. Thus, we obtain the 1D energy signal from the sequence of 2D thermal frames. The signal may contain high frequency noise due to imperfections in the tracking algorithm. We use a Fast Fourier Transformation (FFT)-based noise-cleaning algorithm to suppress such noise.

The tracker is based on particle filtering driven by a probabilistic template mechanism with spatial and temporal smoothing components. The spatial smoothing component is based in part on a fuzzy mask (Matte) [20], which was originally developed for segmentation purposes in visual imaging. The strong point of Matte for the problem at hand is that it is based on pixel dependence (spatial smoothness). Indeed, there is spatial smoothness in thermophysiological imagery of the face. Muscular areas are relatively homogeneous and so are vascular areas. This is in contrast to the pixel independence assumption of appearance modeling [21], which is not realistic here. We have also introduced a temporal smoothness assumption by modifying the Matte formula accordingly. This assumption holds true for appropriately small time window and reduces oscillation.

More precisely, the pixel $T_t(i)$ of the updated template at time t arises as a weighted sum of the previous template $T_{t-1}(i)$, which was estimated at time $t-1$, and the perinasal pixel $\mathcal{F}_t(i)$ from the current frame at time t:

$$\mathbf{T}_t^i = \alpha_t^i \mathbf{T}_{t-1}^i + (1-\alpha_t^i)\mathcal{F}_t^i. \quad (6)$$

The weight $\alpha_t(i)$ is being determined by the spatiotemporal Matte value; this computation is detailed in [19].

The tracker is an important adjunct to the perspiration computation methods in field applications where noticeable facial motion is present. Please note that we have made a number of design choices to facilitate the tracking operation; the most important was the emphasis we paid on spatial detail. We used a powerful lens (100 mm) and placed the camera system close to the subject (~ 8 ft) so that his/her face covers almost the entire field of view. As a result, the small perinasal region is projected into a substantial apparent region on the image plane, providing adequate statistical support for the tracker and the perspiration quantification algorithms.

A shortcoming of this design choice is that the subject's face may go out of the field of view if she/he makes substantial head moves. Thankfully, for the targeted applications this is not an issue because the subject is focused either on a computer screen or a custom simulator. However, even small head motions present challenges as they are random, nonlinear, and translate to substantial pixel-level traversals within fractions of a second. The use of a particle filter tracker, which is a fast and nonlinear mechanism, effectively addresses these challenges.

Depending on the type of motion involved in the target application, quality control may be needed to eliminate tracking errors. Thankfully, it is easy to detect tracking induced errors in thermophysiological signals. These correspond to signal points where there are unnatural drops or elevations in the order of tenths of $^\circ$C (or more) within a fraction of a second. This usually indicates that the tracker has failed by moving to a neighboring region (e.g., cheek) with different thermophysiological characteristics; rarely, the lock is lost forever; most often, the lock is reestablished within a couple of seconds. If the lock is lost for good, the operator needs to go back to the appropriate frame in the thermal clip and reposition the tracker to the correct tissue part (perinasal). Then the tracker is left to continue from that point on.

We did not have any catastrophic loss of lock in the field application data set we present in this paper; we had, however, seven transient tracking failures (each lasting 1-3 s). This is a remarkable tracking performance for a thermal recording that totaled 4,423 s. Hence, when the method is used in applications well matched to its capabilities (e.g., laparoscopic training), operator intervention is not necessary. The sparsity and transient nature of tracking errors cannot materially affect the overall results. However, when research rigor is at stake or the application is technically challenging, then operator assistance through a well-designed user-interface is recommended.

3 Experimental and Clinical Results

Three experiments were carried out to investigate the performance of the new methods. In the first experiment, the algorithms were tested on a simulated data set where the perspiration spots were modulated in a controlled manner (Section 3.1). The simulation enabled us to understand the relation between the algorithms' performance and the dynamic behavior of the perspiration spots. The second experiment was carried out in the lab, where orienting responses were invoked on subjects ($n = 18$) via auditory stimuli (Section 3.2). Once validated, the algorithms were used to quantify stress in the context of inanimate surgical training ($n = 24$) (Section 3.3).

For both the lab and field experiments, data were acquired with a Mid-Wave Infrared (MWIR) camera from FLIR (model SC6000) at a constant frame rate of 25 fps. The camera features an indium antimonite (InSb) detector operating in the range 3-5 μm and has a Focal Plane Array (FPA) with maximum resolution of 640×512 pixels. The sensitivity is 0.025°C. The camera was outfitted with a MWIR 100 mm lens $f/2.3, Si:Ge$, bayonet mount from FLIR. It was calibrated with a two-point calibration at 26°C and 34°C, which are the end points of a typical thermal distribution on a human face.

3.1 Simulation Study

In the simulated data study, first we modeled the intensity evolution of a perspiration spot; then, we attempted to capture this intensity evolution by applying the morphology and wavelet-based methods on the simulation data. Controlling the basic perspiration phenomenon facilitated sensitivity analysis of the two methods.

To build the simulation, we used as background the thermal image of a subject's perinasal area when in nonperspiring mode. The size of the background patch was 100×100 pixels. Within the background patch, a perspiration spot was simulated to ascribe to a certain evolution pattern. We determined this pattern by studying emotional perspiration around an orienting event in a randomly selected facial thermal clip from the lab experiment set.

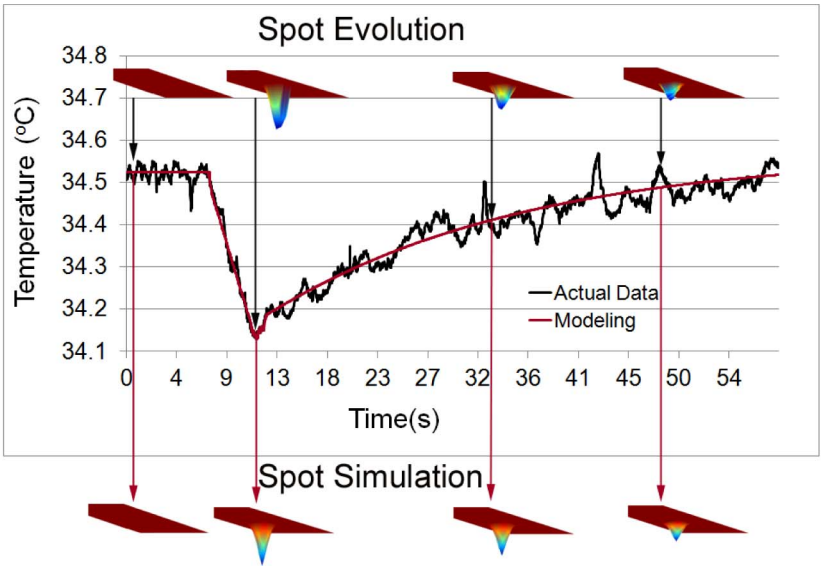

Fig. 4. Ground-truthing of perspiration spot evolution (top part) and resulting modeling (bottom part) around a startle event.

We manually segmented and then computed the mean intensity of a perspiration spot in every frame of the clip. Perspiration spots appear at the onset of an orienting event. Their intensity reaches a culmination point during the arousal period. As this change is found to be nearly impulsive, we use linear fitting to model the onset phase θ_A of perspiration. In the recovery period, the intensity of perspiration spots recedes. As this change is found to be exponential, we use the Laplace distribution to model the recovery phase of perspiration [10].

Specifically, the intensity evolution θ_R of a perspiration spot during recovery can be approximated by

$$\theta_R(t) = \frac{1}{2b_R} exp\left(-\frac{t-\mu}{b_R}\right) \Rightarrow \\ \ln(\theta_R) = \left[\frac{\mu}{b_R} - \ln(2b_R)\right] - \frac{1}{b_R}t, \tag{7}$$

where μ is the location of the culmination point, which is known to us, and b_R is a scale parameter that needs to be estimated. The time t and logarithmic scale $\ln(\theta_R)$ are linearly related. We use the ordinary least squares method to estimate the slope, whose negative inverse is the parameter of interest b_R. We truncate the left side of the Laplace distribution as the recovery phase is at the right side of the culmination point.

Fig. 4 illustrates not only the ground-truthing process (top part), but also the modeling process (bottom part). The signal is actual data, while the fitted curves represent the linear and the Laplace models of the arousal and recovery phases respectively. In simulation, perspiration spots draw mean intensity values from these curves as they evolve on a static patch. These mean values parameterize Normal distributions, which best represent the heat diffusion effect in thermal imagery (see evolving 3D plots in Fig. 4). For the distance (~ 8 ft) and type of lens (100 mm) used, the typical size of the perspiration spot was 5×5 pixels.

We performed the following tests against the simulated data to quantify the sensitivity and performance of the two methods.

3.1.1 Test-1—Reproducibility

We computed the ground-truth perspiration energy signal out of θ_A and θ_R. Then, we extracted nonnormalized perspiration energy signals from the modeled data set according to the morphology and wavelet-based methods. Both signals appear to coincide with the ground-truth approximations. Hence, the methods behave as expected and capture the basic form of the perspiration phenomenon well.

3.1.2 Test-2—Impact of Hot Spot

We reversed the sign of the intensity evolution depicted in Fig. 4 to simulate a hot spot. The morphology algorithm did not localize the hot spot; it correctly produced zero perspiration energy throughout the thermal clip. The wavelet algorithm did localize the hot spot and failed this test. Because the wavelet approach capitalizes on texture oscillation, it is unable to discriminate between hot spots (e.g., skin irritation) and cold spots (i.e., perspiration pores). Hence, one should avoid applying the wavelet algorithm when the skin in the perinasal area has minor irritations.

3.1.3 Test-3—Size of Structure Element

We performed sensitivity analysis regarding the size of the structure element S in the morphology-based approach. We experimented with S sizes in the range 3×3 to 13×13. Table 1 summarizes the mean perspiration

TABLE 1
Simulation Data: Mean Perspiration Energy

Method	Mean-Energy (°C^2)
Morphology (S-3x3)	0
Morphology (S-5x5)	0
Morphology (S-7x7)	0.022
Morphology (S-9x9)	0.022
Morphology (S-11x11)	0.022
Morphology (S-13x13)	0.022

TABLE 2
Simulation Data: Mean Processing Time per Frame (100×100 Pixels)

Method	Time (s)
Morphology (S-3x3)	0.004
Morphology (S-5x5)	0.006
Morphology (S-7x7)	0.009
Morphology (S-9x9)	0.011
Morphology (S-11x11)	0.016
Morphology (S-13x13)	0.021
Wavelet	0.262

energy of the nonnormalized signals for different S sizes. The resulting energy for small S sizes (3×3 or 5×5) is zero. In other words, the morphology algorithm fails to detect the perspiration spot whenever the size of the spot is larger than that of the structuring element. Larger S sizes (7×7 and above) yield the same mean energy value. This is an indication that the mean energy is not affected by the size variation of S as long as S is larger than the perspiration spots.

3.1.4 Test-4—Processing Speed

Table 2 lists the mean processing times for various parameterized versions of the morphology and wavelet algorithms. The algorithms were implemented in Matlab 7.9, on a 2.66 GHz Dell Precision 490 with 3 GB RAM.

The table clearly illustrates that the morphology-based method is computationally inexpensive when compared with the wavelet approach. However, the processing speed increases nonlinearly with the size of the structure element S. Too small S-size and the morphology-based method undersegments the perspiration spots, while too large S-size reduces the processing speed without improving performance. The S size 9×9 pixels was chosen as the optimal option for the experimental scenario that is relevant to this study. This scenario includes subject distance from the camera at 8 ft, a camera focal plane array of 640×512 pixels, and the use of 100 mm lens. For different experimental scenarios, the S size has to be adjusted accordingly, taking into account the optical parameters.

The wavelet algorithm devotes a significant portion (~ 86 percent) of the mean processing time (0.262 s) to filter generation. Hence, one way to improve the computational performance of the wavelet algorithm is to optimize the filter generation code.

3.2 Lab Study

The current standard in real-time measurement of peripheral sympathetic responses is EDA sensing on the fingers. The perinasal imaging method used in this study aims to become the new standard. It has two important advantages: 1) It applies on a more accessible part of the body. 2) It is contact-free and hence has minimal imprint on stress generation. Still, it has to pass a validation check, which could be summarized as follows: "Is the perinasal imaging method equivalent to the finger EDA method?"

To provide an answer to the validation question, we conceived the following experimental design: We recruited

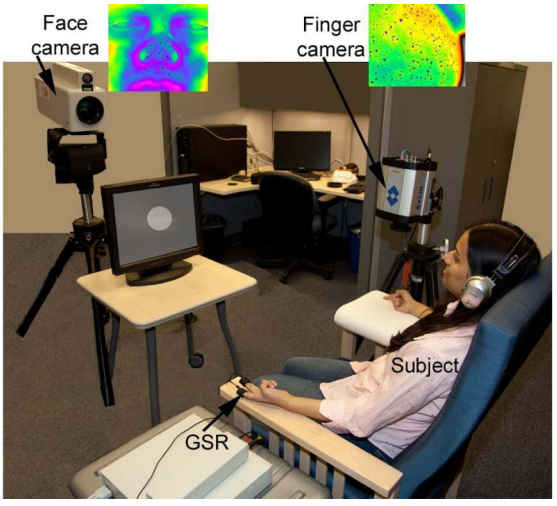

Fig. 5. Lab experimental setup for validation of the Thermal Imaging Method (TIM). The insets show snapshots of the subject's thermo-physiological responses on the perinasal and index finger areas following auditory startle. The black spots in the images indicate activated perspiration pores.

volunteers ($n_V = 18$, 8 males and 10 females) who underwent a controlled stress producing protocol, approved by the local Institutional Review Board (IRB). Repeated orienting responses were invoked using auditory stimuli. The experiment lasted 4 min per subject. After the first minute, a stimulus was delivered and after that two more were delivered, spaced about 1 min apart, resulting in three events. During the experiment, the subjects focused on the simple mental task of counting circles that appeared on a monitor. This amplified their reactions to stimuli.

EDA probes were attached on the subject's left hand index and middle fingers, a thermal imaging sensor aimed at the subject's right hand index finger, and another thermal imaging sensor aimed at the subject's perinasal area (Fig. 5). All three measurement modalities were synchronized and recorded throughout the experimental timeline. This design allows us to examine first if the imaging method (morphology or wavelet-based) correlates with the ground-truth method (i.e., EDA) on the same part of the body (fingers). Additionally, it facilitates examination of the correlation between the perinasal and finger responses.

Exactly the same validation process applies to both the morphology and wavelet-based imaging methods. Hence, in the interest of brevity, we describe the morphology-based case only. The numerical details of the wavelet-based case can be gleaned in Figs. 6b1 and 6b3. Evidently, both imaging methods produce very similar results, which are in agreement with ground-truth.

We start our analysis by finding the location of the maximum for each event (first, second, third) in every signal (EDA-Finger, Thermal-Finger, Thermal-Perinasal). The location of the maximum (max) corresponds to the time the measured phenomenon is at its peak and for this reason we call it Event Peak Time (EPT). If the same maximum value occurs more than once, we consider the earliest. Initially, we are interested in checking if the max locations proposed by the two thermal imaging signals are equivalent to those of EDA or not. Given that the signals are synchronized, we can

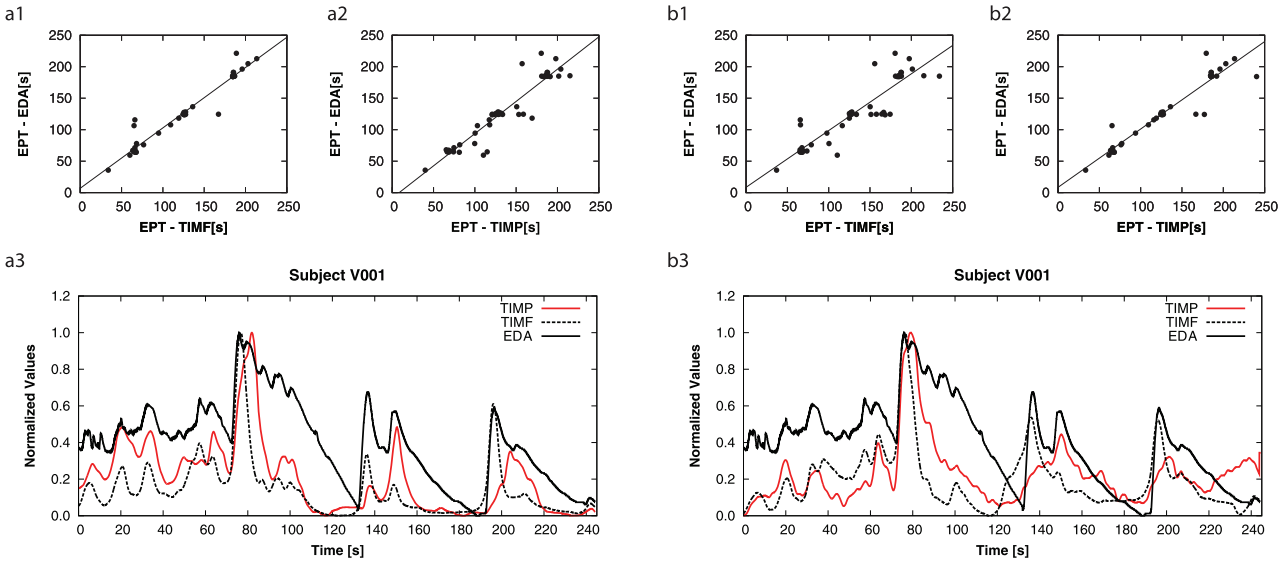

Fig. 6. Morphology validation. (a1) Scatterplot that indicates strong linearity between event peak times in the EDA and Thermal Imaging Measurements on the Finger (TIMF)—$r = 0.974$. (a2) Scatterplot that indicates strong linearity between event peak times in the EDA and Thermal Imaging Measurements on the Perinasal (TIMP)—$r = 0.943$. (a3) EDA, TIMF, and TIMP signals for subject V-001 from the lab validation set. Wavelet Validation. (b1) Scatterplot that indicates strong linearity between event peak times in the EDA and Thermal Imaging Measurements on the Finger—$r = 0.961$. (b2) Scatterplot that indicates strong linearity between event peak times in the EDA and Thermal Imaging Measurements on the Perinasal—$r = 0.914$. (b3) EDA, TIMF, and TIMP signals for subject V-001 from the lab validation set.

consider that EDA is paired each time with one of the two imaging measurements. Hence, we will perform a paired T-test to check whether the EDA and each of the thermal imaging measurements have statistically equivalent recognition of the peak of the phenomenon. Given that events are about 60 s apart, we study the statistical equivalence in detecting the peak separately for each event.

The null hypothesis is that the two populations have equal means and the alternative hypothesis is that there are differences in the means (greater or less than). Decisions based on p-values are drawn as follows:

- $P < 0.05$—Decision: We have evidence to reject the null hypothesis.
- $P > 0.05$—Decision: We do not have evidence to reject the null hypothesis.

For EDA versus Thermal Imaging Measurement on Finger (TIMF) we find $P > 0.05$ for all three events. In other words, EDA and TIMF have equivalent event detection times. This establishes that probe-based and imaging-based measurements on the same part of the body (i.e., finger) can be used interchangeably. For EDA versus Thermal Imaging Measurement on Perinasal (TIMP) we find that $P < 0.05$ for the first two events. In other words, EDA and TIMP have different detection times for the first two events. In fact, mean EPT latency in TIMP lags ~ 9 s with respect to mean EPT latency in EDA. Still, the linearity between EPT-EDA and EPT-TIMP (see Fig. 6a2) is as strong as the linearity between EPT-EDA and EPT-TIMF (see Fig. 6a1). Therefore, TIMP is predictive of sympathetic responses to the same degree as EDA. Fig. 6a3 shows the EDA, TIMP, and TIMF signals for subject V-001 from the lab experimental cohort. This is a representative case and provides a vivid visualization of the agreement (EDA versus TIMF) or consistency (EDA versus TIMP) of the signal pairs.

The consistent delay pattern of TIMP with respect to EDA responses breaks down in Event 3, where EPT-TIMP times become equivalent to EPT-EDA times ($P > 0.05$). This may be the direct effect of habituation, as responses to the last stimulus are being smoothed to a considerable degree.

It is intriguing that in nonhabituating mode, physiology clearly prioritizes responses in favor of tactile sensing. One could only wonder if in primates with much more developed nasal sensing than humans [22], the neurophysiological prioritization scheme differs.

Please note that the thermal map on the nasal area (which borders the perinasal) is modulated by the semi-periodic effect of breathing. This modulation is isotropic, but at a different scale than the perspiration one. Hence, the corresponding breathing signal can naturally be recovered within the multiresolution wavelet context. Fig. 7 vividly depicts the point for subject V-012 of the lab validation set. It is telling how the intensity and frequency of breathing increases as the experiment unfolds, indicating the adrenergic response to stress (versus the cholinergic that was mainly studied in this paper). This result highlights the broader potential of the wavelet-based method.

3.3 Field Study

Armed with the validated imaging methodologies we developed, we attempted to gauge their practical power in studying stress of surgeons while training in an inanimate laparoscopic skills facility. This is one of the few stress studies that were performed in naturally occurring stress environments (in-situ) thanks to the advantages afforded by the proposed methods. It would have been prohibitive to carry out such a study with fMRI and quite challenging with EEG sensing. Also, it would have been a problem to use EDA sensing in the traditional finger location, although conceivably, EDA sensing could have been attempted in an alternate location (e.g., wrist).

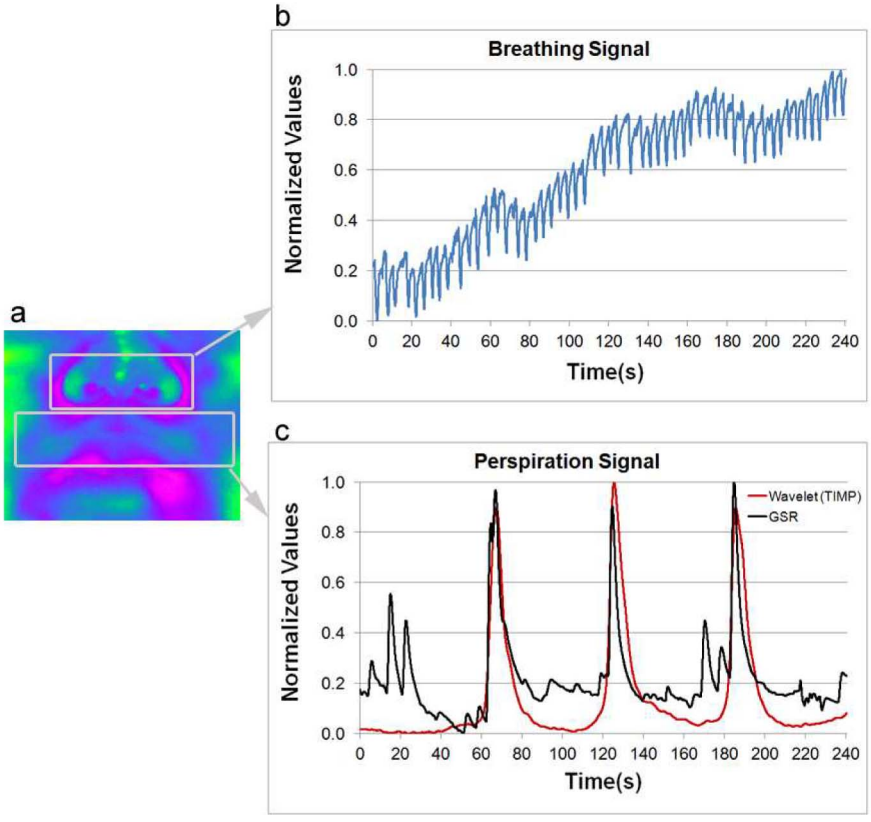

Fig. 7. (a) Thermophysiological facial map of subject V-012 in the beginning of the startle experiment, with virtual probes delineated on the nasal and perinasal areas. (b) and (c) Extraction of the breathing and perspiratory signals via the application of the same isotropic wavelet method (at different scales) on the nasal and perinasal areas, respectively.

We recorded perinasal thermophysiological data from 24 surgeons while they were executing training drills in a laparoscopic simulator box (see Fig. 8). The set included six novice (age 25.3 ± 2.1) and 18 experienced (age 37.3 ± 8.4) surgeons. The drill on which these surgeons engaged was intracorporeal suture. The goal was to perform the drill as fast as possible without committing any errors. The proficiency time established by the American Board of Surgeons for this task is 112 s. A surgical instructor was supervising training and was recording time elapsed and errors committed. The study was designed and executed according to an Institutional Review Board approved protocol.

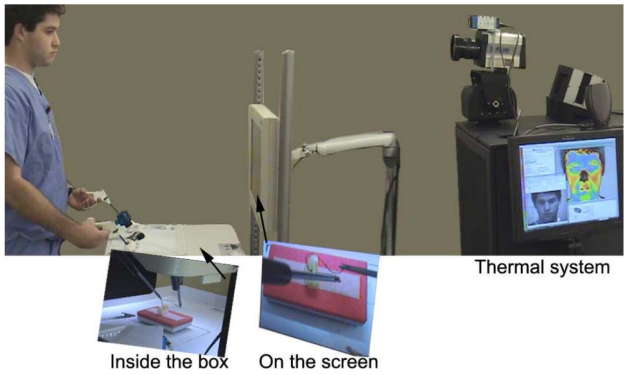

Fig. 8. Clinical set-up. A novice surgeon performs intracorporeal suturing in the surgical simulation box while his face is being thermally imaged. The operation is endoscopically driven.

Prior to commencing task execution the surgeons went through a 3 min break during which they perused serene landscapes on a computer screen. This was meant to serve as a dissociation period between the training session and the surgeons' previous engagements, whatever these might have been. If the dissociation period were longer, it may have had the characteristics of a true baseline. Due to the tight schedule of surgeons, however, this was not possible. For this reason, we consider this 3 min break as a pseudobaseline period. Surgeons were imaged during the pseudobaseline period in the same way as during task execution.

From each clip the perspiration signals were extracted with the two proposed methods, that is, morphology and 2D isotropic wavelets. It would have been of interest to check if the two methods produced signals similar to the ground-truth, as we did in the lab study. Unfortunately, there is no ground-truth data available in this study because we could not attach EDA sensors on the surgeons' fingers, Additionally, no one could be absolutely sure about the stress triggers as they are naturally and not artificially produced. However, we noticed that excitations manifested in the perinasal signals usually coincide with errors performed during task execution. In other words, the challenges presented in error recovery appear to act as natural stimuli.

A different analysis method was adopted for the field study with respect to the lab study. One axis of analysis was qualitative and examined if the respective signals produced by the morphology and wavelet methods follow the same pattern and correspond well to perspiration visualization.

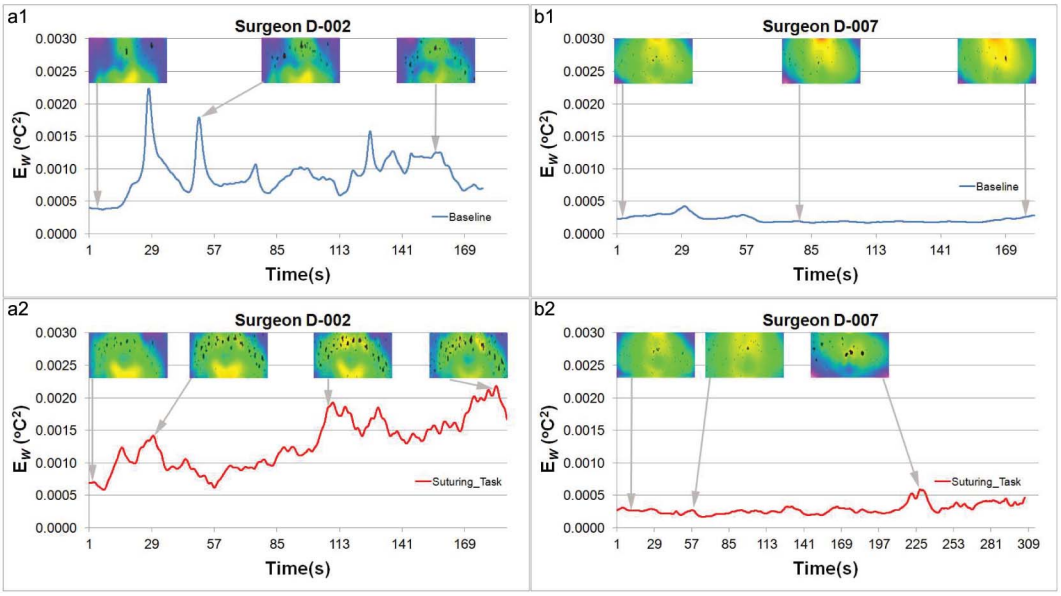

Fig. 9. Perinasal signals of a novice surgeon. (a1) Before task execution, indicating an agitated state. (a2) During task execution, where the surgeon committed five errors (needle drops) accompanied by neurophysiological responses that manifest as "bumps" in the signal. Perinasal signals of an experienced surgeon. (b1) Before task execution, indicating a calm state. (b2) During task execution, where about 200 s into the task, the surgeon faced difficulties in tying the knot (see signal "bump").

This is an indication that both methods consistently measure the expected physiological variable.

Fig. 9 illustrates the thermal signals for Surgeon D-002 (novice) and Surgeon D-007 (experienced). It clearly demonstrates a qualitative agreement between the thermal visualization on the perinasal area (insets) and the thermal perspiration signals. Specifically, fewer and less intense perspiration spots coincide with lows in the signals, while more numerous and intense spots coincide with highs in the signals. The latter typically occur when the surgeon faces difficulties during task execution.

A second axis of analysis is to check if conclusions afforded by these signals verify rational hypotheses about expected stress levels. Then, there would be strong circumstantial evidence that the variable being measured (i.e., perinasal perspiration) is associated with physiological stress. Finally, coupling these analysis axes with the results of the lab experiments and the literature findings [10] would render the evidence airtight.

The main research hypothesis is that among the different levels of surgeons the respective perspiration signals (of the same method) are different in the mean sense. Specifically, the assumption is that the less experienced a surgeon is the higher the expected stress level during task execution, which leads to stronger neurophysiological responses in the perinasal area. Please note that all other variables in the experiment are controlled; for example, all surgeons perform exactly the same drill.

For each signal $\mathbf{E}_M$ extracted via the morphology-based method from subject D_i, we compute the mean perspiration energy $\overline{\mathbf{E}}_M(i)$. Similarly, we compute the mean perspiration energy values $\overline{\mathbf{E}}_W(i)$ corresponding to the wavelets-based method (see Table 3).

Figs. 10a and 10b show the box-plots of the mean perspiratory signal values, as computed through the morphology and wavelet-based methods respectively, grouped according to surgical levels of expertise. Experienced surgeons (Experience $= 1$) have substantially more subdued responses (and thus stress) than novice surgeons (Experience $= 0$). In order to run the ANOVA test, we needed to have equal variances for the two populations. For this

TABLE 3
Clinical Data: Mean Energy Values for Morphology and Wavelet-Based Perspiration Signals

Subject	Gender	Experience	$\overline{\mathbf{E}}_M(i)$ (°C^2)	$\overline{\mathbf{E}}_W(i)$ (°C^2)
D-001	M	1	0.002221	0.000674
D-002	M	0	0.009235	0.001112
D-003	F	1	0.000860	0.000775
D-005	M	1	0.003499	0.000626
D-006	F	1	0.000583	0.000398
D-007	M	1	0.001755	0.000577
D-008	M	1	0.001634	0.000502
D-010	F	1	0.001138	0.001806
D-011	M	1	0.000454	0.000398
D-013	M	1	0.004078	0.002206
D-015	M	1	0.001981	0.001188
D-017	M	1	0.000530	0.000663
D-020	M	0	0.002600	0.010636
D-022	M	0	0.001020	0.001650
D-023	M	0	0.002239	0.001236
D-025	F	0	0.002913	0.000640
D-027	F	0	0.001627	0.002733
D-102	M	1	0.000891	0.001494
D-104	M	1	0.000414	0.000870
D-105	F	1	0.001360	0.001561
D-107	M	1	0.000524	0.000681
D-109	M	1	0.000580	0.003458
D-110	M	1	0.000877	0.000674
D-111	M	1	0.001104	0.000322

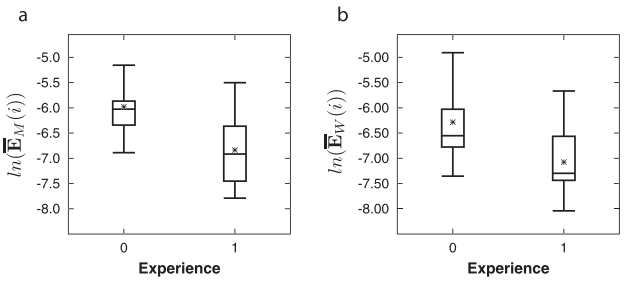

Fig. 10. Box-plots of mean perspiration responses computed via (a) the morphology-based and (b) the wavelet-based methods for the two levels of surgical expertise. Surgeons with less experience ($\text{Experience} = 0$) have higher perspiration responses perinasally, believed to be related to their greater stress and workload performing the task.

reason, we transformed the responses to the natural logarithm of morphology-based mean energy $\ln \overline{\mathbf{E}}_M(i)$ and wavelet-based mean energy $\ln \overline{\mathbf{E}}_W(i)$ respectively—see Figs. 10a and 10b. The null hypothesis is that there are no differences between novice and experienced surgeons. The p-values are 0.017 and 0.032 for the morphology and wavelet cases respectively; thus, both methods report statistically significant differences of the mean perspiratory responses between novice and nonnovice surgeons.

It is worth mentioning that there were significant differences in the mean perinasal responses between the novice and experienced cohort during the pseudobaseline period (analysis of variance, $P < 0.05$ for both the morphology and wavelet-based methods). Specifically, novice surgeons were coming in with higher perinasal activity levels than those of experienced surgeons, which is what we had predicted with higher stress. Task execution simply pushed these disparate stress levels higher.

Please note that the experimental protocol tagged on true training and evaluation sessions that were graded by a surgical educator and had some formality. In light of this, the pseudobaseline results make sense and correlate with personal experiences. In formal exams early in our student lifetime, and especially when we were not well prepared, stress did not start the moment we started writing the answers. We rather felt it to a significant degree a few minutes before the beginning of the exam, while we were waiting to receive the questions (anticipatory arousal).

4 Discussion

We have described two methods for quantifying perspiratory responses on the perinasal area through thermal imaging. These responses are sympathetically driven and hence are indicative of stress elevation in certain contexts. One method is based on morphology and the other on spatial isotropic wavelets. The architecture of the methods is driven by the characteristics of the underlying physiological phenomenon. The morphology method is made out of standard (but fitting) components found in the literature. The isotropic wavelet method is not only fitting to the problem, but is also quite novel, as its filter has been developed from scratch. Both methods require the support of a facial tracker. In this paper, we used a tracker based on spatiotemporal smoothing [19] with good results. Other reliable facial trackers, however, could be equally effective.

We validated the algorithmic methods in controlled lab experiments against the clinical standard, which is EDA sensing on the fingers. We also analyzed their sensitivity and performance by conducting simulation studies. Both methods appear to perform on par. The morphology-based method, however, is more computationally efficient than the wavelet-based method and should be preferred in practice. The wavelet-based method becomes highly competitive when one wants to study both cholinergic (i.e., perspiration) and adrenergic (e.g., breathing) responses to stress onset [23]. Please note that if one uses the morphology-based method to extract the perspiratory response in this case, she/he would need an entirely different algorithm (i.e., wavelets) to run in parallel in order to extract the breathing signal.

To demonstrate the application potential of these methods, we used them in a field study where stress occurred naturally during surgical training sessions restricted to a laparoscopic simulator box. The perspiration signals extracted via the two methods continued to be in agreement and accurately matched highs and lows in the perspiration visualization afforded via the thermal imagery. Furthermore, the mean perspiration signal (energy) responses were subjected to the ANOVA test. The outcome confirmed that the perinasal responses of novice surgeons were significantly higher than those of experienced surgeons. Therefore, in the absence of other differentiating factors, neurophysiological signals on the face during standardized surgical training could potentially be used as an efficacy measure. Although further research is required on this matter, it is an intriguing concept with broad implications to this and other field applications.

One important consideration for the field study is the effect of age on the observed neurophysiological responses. Indeed, there is some support in the literature regarding the diminution of electrodermal (EDA) responses in older people. Typically, these studies [24] refer to comparisons between very young adults (mean age, 20 years) versus very old adults (mean age, ~ 70 years). In our case, age differences are not as dramatic (early middle age versus young adults). It is doubtful that these moderate age differences alone account for the highly significant differences in the perinasal signals between the two groups of surgeons. In fact, we have suggestive evidence that this is likely not the case, as experienced surgeons commit errors in a few instances and transiently produce perinasal responses comparable to the novice cohort (Fig. 9).

Unfortunately, we did not get true baseline measurements (e.g., after a really long break) due to practical constraints. What is important here, however, is that the neurophysiological disparity between the two surgeon groups grew larger during tasking (see Section 3.3), a clear indicator of the anisotropic stress effect of challenging action. This is a defining result in the absence of any other differential factors. Specifically, all surgeons had full days with few (if any) breaks. All training and evaluation took place in the same facility with exactly the same environmental conditions. Surgeons remained in this facility just for the duration of the training protocol; no one came in well in advance of the appointment time and no one lingered after the protocol's completion.

Quantification of stress levels in context is important in usability studies [25], human performance studies [26], and recently even in marketing studies [27]. Henceforth, the proposed imaging methods can find an array of applications in affective computing. In fact, the totally unobtrusive nature of perinasal imaging may be vital in certain affective studies (such as the case of laparoscopic training), where other physiological stress measurement methods are less appealing or impossible.

One should be mindful, however, of the perinasal imaging methods' limitations: 1) They depend on an expensive sensor and cannot be used in great numbers. 2) They are locally tied. 3) They cannot operate if the perinasal area is covered. For example, the methods cannot be employed in a real operating room where surgeons wear masks. Luckily, in inanimate surgical training, which was the case in our field study, such masks are not worn.

The arrival of the Q sensor (bracelet EDA) [28] opens new possibilities in affective physiological sensing. The sensor is relatively low cost and a multitude of them can be used in each stress study. It would be ideal, for example, in a stress study of class students while they take exams. However, when the stress study can be performed on one person at a time and in a set locale, we find that the perinasal method becomes highly attractive. This is due not only to its noncontact nature, but also due to the instant qualitative verification that it provides thanks to its visual form (density of perspiration pores against extracted signal). In conclusion, we find that this emerging generation of unobtrusive methods and systems, exemplified by the perinasal channel and the Q sensor, will provide affective researchers with a powerful set of tools to choose from, depending on their aims and applications.

Please note that the perinasal imaging methods should never be used outside a well-defined context. Perinasal responses (and transient perspiratory responses in general) are sympathetic in nature, merely indicating arousal, which could be negative (distress) or positive (eustress). For example, in a pleasant situation, the subject would produce responses similar to the ones produced during surgical training. This nonspecificity is ameliorated only within a well-defined stimulative context, such as the orienting stimuli or challenging surgical drills used in our studies.

Acknowledgments

This material is based upon work supported by US National Science Foundation (NSF) award IIS-0812526 entitled "Do Nintendo Surgeons Defy Stress?" It was also supported in part by a contract from the US Department of Defense Technical Support Working Group (TSWG) entitled "Thermal Action Coding System" and NSF award DMS-0915242. The authors acknowledge the help of Dr. Thirimachos Bourlai and Ms. Anitha Mandapati.

References

[1] J.R. Hubbard and E.A. Workman, *Handbook of Stress Medicine: An Organ System Approach.* CRC Press, 1998.

[2] C. Spielberger, R. Gorsuch, and R. Edward, *Manual for the State-Trait Anxiety Inventory.* Consulting Psychologists Press, 1970.

[3] D. Watson, L. Clark, and A. Tellegen, "Development and Validation of Brief Measures of Positive and Negative Affect: The Panas Scales," *J. Personality and Social Psychology,* vol. 54, no. 6, pp. 1063-1070, 1988.

[4] K. Bortnik, L. Henderson, and P. Zimbardo, "The Shy Q, a Measure of Chronic Shyness: Associations with Interpersonal Motives, Interpersonal Values and Self-Conceptualizations," *Proc. 36th Ann. Conf. Assoc. for the Advancement of Behavior Therapy,* 2002.

[5] P. Ekman and E. Rosenberg, *What the Face Reveals: Basic and Applied Studies of Spontaneous Expression.* Oxford Univ. Press, 2005.

[6] B.S. McEwen, "Physiology and Neurobiology of Stress and Adaptation: Central Role of the Brain," *Physiological Rev.,* vol. 87, pp. 873-904, 2007.

[7] C. Cohen, R. Kessler, and L. Gordon, *Measuring Stress: A Guide for Health and Social Scientists.* Oxford Univ. Press, 1978.

[8] A. Uncini, S. Pullman, R. Lovelace, and D. Gambi, "The Sympathetic Skin Response: Normal Values, Elucidation of Efferent Components and Application Limits," *J. Neurological Sciences,* vol. 87, pp. 299-306, 1988.

[9] M.-Z. Poh, S. Swenson, and R. Picard, "A Wearable Sensor for Unobtrusive, Long-Term Assessment of Electrodermal Activity," *IEEE Trans. Biomedical Eng.,* vol. 57, no. 5, pp. 1243-1252, May 2010.

[10] D. Shastri, A. Merla, P. Tsiamyrtzis, and I. Pavlidis, "Imaging Facial Signs of Neurophysiological Responses," *IEEE Trans. Biomedical Eng.,* vol. 56, no. 2, pp. 477-484, Feb. 2009.

[11] F. Martini, *Fundamentals of Anatomy and Physiology,* sixth ed., pp. 170-171. Benjamin Cummings, 2004.

[12] O. Lupi, "Ancient Adaptations of Human Skin: Why Do We Retain Sebaceous and Apocrine Glands," *Int'l J. Dermatology,* vol. 47, pp. 651-654, 2008.

[13] P. Soille, *Morphological Image Analysis: Principles and Applications.* Springer, 2003.

[14] X. Bai and F. Zhou, "Analysis of New Top-Hat Transformation and the Application for Infrared Dim Small Target Detection," *Pattern Recognition,* vol. 43, no. 6, pp. 2145-2156, 2010.

[15] C. Hendriks and L. van Vliet, "A Rotation-Invariant Morphology for Shape Analysis of Anisotropic Objects and Structures," *Proc. Fourth Int'l Workshop Visual Form,* pp. 378-387, 2001.

[16] J. Romero, S. Alexander, S. Baid, S. Jain, and M. Papadakis, "The Geometry and the Analytic Properties of Isotropic Multiresolution Analysis," *Advances in Computational Math.,* vol. 31, pp. 283-328, 2009.

[17] S. Jain, M. Papadakis, and E. Dussaud, "Explicit Schemes in Seismic Migration and Isotropic Multiscale Representations," *Radon Transforms, Geometry, and Wavelets,* E. Grinberg, D. Larson, P. Jorgensen, P. Massopust, G. Olafsson, E. Quinto, and B. Rubin, eds., pp. 177-200, Am. Math. Soc., 2008.

[18] M. Papadakis, B. Bodmann, S. Alexander, D.V. MD, S. Baid, A. Gittens, D. Kouri, S.G. MD, S. Jain, J. Romero, X. Li, P. Cherukuri, D. Cody, G.W.G. MD, I.A. MD, J. Conyers, and S. Casscells, "Texture-Based Tissue Characterization for High-Resolution CT-Scans of Coronary Arteries," *Comm. Numerical Methods in Eng.,* vol. 25, pp. 597-613, 2009.

[19] Y. Zhou, P. Tsiamyrtzis, and I. Pavlidis, "Tissue Tracking in Thermo-Physiological Imagery through Spatio-Temporal Smoothing," *Proc. 12th Int'l Conf. Medical Image Computing and Computer-Assisted Intervention,* pp. 1092-1099, 2009.

[20] A. Levin, D. Lischinski, and A. Weiss, "A Closed Solution to Natural Image Matting," *IEEE Trans. Pattern Analysis and Machine Intelligence,* vol. 30, no. 2, pp. 228-242, Feb. 2008.

[21] A. Jepson, D. Fleet, and T. El-Maraghi, "Robust Online Appearance Models for Visual Tracking," *IEEE Trans. Pattern Analysis and Machine Intelligence,* vol. 25, no. 10, pp. 415-422, Oct. 2003.

[22] R. Sapolsky, "The Olfactory Lives of Primates," *Virginia Quarterly Rev.,* vol. 82, no. 2, pp. 86-90, 2006.

[23] R. Seeley, T. Stephens, and T.P., *Anatomy and Physiology,* fifth ed., pp. 555-556, McGraw Hill, 2003.

[24] J. Botwinick and C. Kornetsky, "Age Differences in the Acquisition and Extinction of the GSR," *J. Gerontology,* vol. 15, no. 1, pp. 83-84, 1960.

[25] T. Lin, M. Omata, W. Hu, and A. Imamiya, "Do Physiological Data Relate to Traditional Usability Indexes?" *Proc. 17th Australia Conf. Computer-Human Interaction,* pp. 1-10, 2005.

[26] J. Levine, I. Pavlidis, L. MacBride, Z. Zhu, and P. Tsiamyrtzis, "Description and Clinical Studies of a Device for the Instantaneous Detection of Office-Place Stress," *Work: A J. Prevention, Assessment and Rehabilitation,* vol. 34, no. 3, pp. 359-364, 2009.

[27] N. Lee, A. Broderick, and L. Chamberlain, "What Is 'Neuromarketing'? A Discussion and Agenda for Future Research," *Int'l J. Psychophysiology,* vol. 63, no. 2, pp. 199-204, 2007.

[28] R. Fletcher, K. Dobson, M. Goodwin, H. Eydgahi, O. Wilder-Smith, D. Fernholz, Y. Kuboyama, E. Hedman, M.-Z. Poh, and R. Picard, "iCalm: Wearable Sensor and Network Architecture for Wirelessly Communicating and Logging Autonomic Activity," *IEEE Trans. Information Technology in Biomedicine,* vol. 14, no. 2, pp. 215-223, Mar. 2010.

Dvijesh Shastri received the BE degree in electrical engineering from Sardar Patel University, India, in 1997, the MS degree in computer Science from Wright State University in 2001, and the PhD degree in computer science from the University of Houston in 2007. His research interests include image/signal processing, computational psychophysiology, and pattern recognition. His work has been supported by the US Department of Defense. He is an assistant professor at the Department of Computer and Mathematical Sciences at the University of Houston, Downtown. He is a member of the IEEE.

Manos Papadakis received the doctoral degree in mathematics from the University of Athens, Greece. He is an associate professor in the Department of Mathematics at the University of Houston and his interests include wavelet analysis, frame theory, biomedical image analysis, and seismic imaging. The primary focus of his research is the elimination of errors in computer vision applications resulting from the directional preference of 1D filter designs. He and his collaborators propose that the best antidote to this is the use of isotropic filtering methods, treating all directions equally and enabling the handling of multidimensional data sets in their original dimensionality.

Panagiotis Tsiamyrtzis received the BS degree in mathematics from the Aristotle University of Thessaloniki, Greece, and the MS and PhD degrees in statistics from the University of Minnesota, where he served as a visiting faculty member in the School of Statistics in Fall 2000. In 2004, he joined the Department of Statistics, Athens University of Economics and Business, where he is currently an assistant professor. His research interests include statistical aspects of computer vision problems, statistical process control, and applications of Bayesian statistics. He was the recipient of the Best Student Paper Award and Best Contributed Paper at the 2000 Joint Statistical Meetings of the Risk Analysis Section of the American Statistical Association. He also received the Best Talk Award at the 2007 Annual Conference of the European Network for Business and Industrial Statistics.

Barbara Bass received the BS degree from Tufts University (summa cum laude) in 1975 and the MD degree from the University of Virginia Medical School in 1979. She completed her general surgery residency at George Washington University and her gastrointestinal surgical research fellowship at the Walter Reed Army Institute of Research. Her research interests include surgical quality and outcomes as well as surgical education policy and innovation. She is a senior director and past chair of the American Board of Surgery. She sits on the editorial boards of several journals, including *Annals of Surgery* and *Surgery*. She holds the John F. and Carolyn Bookout Distinguished Endowed Chair of Surgery at the Methodist Hospital, she is the director of the Methodist Institute for Technology, Innovation and Education (MITIE), and is a professor of surgery at Weill Medical College of Cornell University

Ioannis Pavlidis received the BE degree in electrical engineering from Democritus University of Thrace, Xanthi, Greece, in 1987, the first MS degree in robotics from the University of London, United Kingdom, in 1989, and the second MS degree and the PhD degree in computer science from the University of Minnesota in 1995 and 1996, respectively. Currently, he is the Eckhard-Pfeiffer Professor of Computer Science and the director of the Computational Physiology Laboratory at the University of Houston. His research has been supported by multiple sources, including the US National Science Foundation, the US Department of Defense, and corporations. He is the author of many scientific articles on computational physiology and affective computing. He is well known for his work on facial signs of stress, which first appeared in *Nature* and *Lancet*. He is a senior member of the IEEE.